## PAPER

Check for updates

# Self-assembly of hierarchical porous structure for stretchable superhydrophobic films by delicately controlling the surface energy†

Shuhan Hou,‡[a] Insub Noh, [iD] ‡[b] Meng Yue,[a] Yanbin Wang, [iD] *[a] Hyung Do Kim,*[b] Hideo Ohkita [iD] *[b] and Biaobing Wang*[a]

Herein, thermoplastic polyurethane (TPU) was not only used as the means of attaching modified silica (m-SiO$_2$), but was also used as a flexible polymer substrate combining with poly(amide−imide) (PAI) for improving the robustness of stretchable superhydrophobic films by self-assembly. m-SiO$_2$ floated up and TPU sank down in the superhydrophobic coating layer while TPU floated up and PAI sank down in the PAI−TPU stretchable substrate layer by delicately controlling the surface energies of the materials ($\gamma_{PAI} > \gamma_{TPU} > \gamma_{m\text{-}SiO_2}$). With this strategy, the two layers penetrated into each other, and the compatibility between the superhydrophobic coating and polymer substrate was improved due to the same component of TPU, which made m-SiO$_2$ firmly attach to the stretchable substrate and uniformly disperse into the PAI−TPU substrate. In addition, during the up−down process, a hierarchical porous structure with robust microscale bumps was formed, which offered a stable Cassie state. As expected, the PAI−TPU/m-SiO$_2$ superhydrophobic film was highly stretchable, and can bear 2000 cycles of stretching−releasing (0% → 30% → 0%) without sacrificing its superhydrophobicity. The tight adhesion between the decorated m-SiO$_2$ and stretchable substrate rendered outstanding mechanical robustness with resistance to sandpaper abrasion, knife-scuffing, ultrasonic treatment, and hot-water jet impact. The PAI−TPU/m-SiO$_2$ superhydrophobic surface also showed excellent durability when exposed to acid−base immersing, cooling or heating, and UV irradiation. Furthermore, the PAI−TPU/m-SiO$_2$ superhydrophobic surface possessed excellent self-healing, and icephobic properties. For practical application, PAI−TPU/m-SiO$_2$ stretchable superhydrophobic films were applied as water-proof covers for curved surfaces, or served as a self-cleaning coating. These versatile features demonstrated a simple and convenient method to fabricate stretchable superhydrophobic surfaces with multi-functionality.

## 1. Introduction

Recently, stretchable superhydrophobic surfaces have been widely used in wearable electronics, and mechanically sensitive sensors due to their outstanding properties of self-cleaning and being water-proof.[1–3] In general, stretchable superhydrophobic surfaces are composed of a flexible substrate and superhydrophobic coating. For the flexible substrates, they always suffered

[a] *School of Materials Science and Engineering, Changzhou University, Changzhou 213164, People's Republic of China. E-mail: wangyanbin@cczu.edu.cn, biaobing@cczu.edu.cn*

[b] *Department of Polymer Chemistry, Graduate School of Engineering, Kyoto University, Katsura, Nishikyo, Kyoto 615-8510, Japan. E-mail: hyungdokim@photo.polym.kyoto-u.ac.jp, ohkita@photo.polym.kyoto-u.ac.jp*

† Electronic supplementary information (ESI) available. See DOI: https://doi.org/10.1039/d3ma00794d

‡ S. H. and I. N. contributed equally to this work.

from low elastic modulus or poor tensile strength.[4–6] For example, a series of superhydrophobic surfaces based on polyurethane acrylate as the stretchable substrate were fabricated by Li,[7] it was found that the superhydrophobic property was still kept even after they underwent 1000 cycles of stretching–releasing. Nevertheless, it should be noted that their tensile strengths were as low as about 4.5 MPa. In other words, the resulting stretchable superhydrophobic surfaces were easily broken down even under a small force. For the superhydrophobic coating, SiO$_2$, titanium dioxide (TiO$_2$), zinc oxide (ZnO), and other inorganic nanoparticles were always used to increase the roughness of the stretchable substrate.[8–16] However, it is obvious that the compatibility between these inorganic nanoparticles and polymer substrates is very poor, leading to low interfacial adhesion. Thus, the superhydrophobic structures are usually fragile, and the superhydrophobic coatings are easily peeled from the stretchable substrate or destroyed by an external force. For example, Ke *et al.* used polyurethane (PU)

as the stretchable substrate and $SiO_2$ as the coating to fabricate $PU/SiO_2$ hybrid superhydrophobic surfaces.[17] The water contact angle (CA) decreased from 159 to 110° after 300 cm abrasion with a weight load of 200 g. As discussed above, it is still a great challenge to fabricate stretchable superhydrophobic films with good mechanical properties and high durability.

Constructing hierarchical roughness on two length scales has been considered to be an effective approach to enhance mechanical robustness and durability of superhydrophobic surfaces.[18–20] This is because such morphology can produce robust microscale bumps to protect the fragile nanoscale roughness that is superimposed on the larger pattern. For example, hierarchical micro/nanostructures were achieved by Dai using magnetic field-assisted *in situ* microsilica formation, and the subsequent swelling process to decorate $SiO_2$ nanoparticles onto the prepared microstructures.[21] The unique hierarchical structure gave the superhydrophobic surfaces excellent robustness: their superhydrophobic property was still maintained even after they were subjected to lots of durability tests including finger rubbing, ultrasonic treatment, high-speed water jet, and so on. However, manufacturing hierarchical micro/nanostructures is often accompanied by complicated procedures or expensive equipment. Although some simple approaches such as spraying were proposed to construct hierarchical structures,[22–25] it often led to an irregular arrangement of the inorganic nanoparticles during the solvent evaporation, and thus gave rise to poor repeatability. On the other hand, it has been reported that poly(amide–imide) (PAI) as one kind of high performance polymer, not only possesses excellent mechanical properties and high thermal stability like polyimide (PI), but also has good processability like polyamide (PA),[26–30] which can be blended with other soluble polymers with any ratio to control the rigidity and flexibility of the hybrid substrate. In other words, PAI is a good candidate for improving the mechanical properties of stretchable superhydrophobic surfaces.

In this study, an ingenious strategy was proposed to prepare stretchable superhydrophobic surfaces with good mechanical properties and durability using a simple spraying method. Intentionally, three materials (PAI, TPU, and $m-SiO_2$) with different surface energies were selected; the substrate of PAI–TPU hybrid materials gave high tensile strength and good elasticity, and the coating of $m-SiO_2$ decorated with TPU intertwined with the stretchable substrate driven by their surface energy difference, gave high mechanical robustness and durability. Meanwhile, the self-assembly rendered hierarchical porous structures and further improved the mechanical robustness and durability. The self-healing and icephobic properties were also investigated using $O_2$ plasma etching and heating treatments, and icing delay tests, respectively. With the intrinsic flexibility, the fabricated PAI–TPU/$m-SiO_2$ stretchable superhydrophobic films were applied as water-proof covers for complex/curved surfaces, or served as a self-cleaning coating.

## 2. Results and discussion

### 2.1 Design and fabrication of stretchable superhydrophobic surfaces

To fabricate the stretchable superhydrophobic films, a rigid polymer (PAI) was designed as shown in Fig. S1 (ESI†), and the details of the synthetic procedure are described in the supplementary information.† The chemical structure was confirmed using $^1H$ NMR and FTIR spectra as shown in Fig. S2 and S3 (ESI†). Encouragingly, the designed PAI in this study exhibits good solubility, and can be dissolved into pyridine, *N*-methyl-pyrrolidone (NMP), and *m*-cresol at room temperature. When it is heated, it can also be dissolved into *N,N*-dimethylformamide (DMF) and tetrahydrofuran (THF). Furthermore, the inherent viscosity of the PAI was determined to be 0.75 dl $g^{-1}$ using NMP at room temperature, suggesting the molecular weight of PAI is reasonable high. As a result, PAI gave a high tensile strength of 55.6 MPa. An elastic polymer (TPU) with an elongation at break of about 1000% was selected. As shown in Fig. 1a, the hybrid alloy gave a strong and tough substrate with a tensile strength
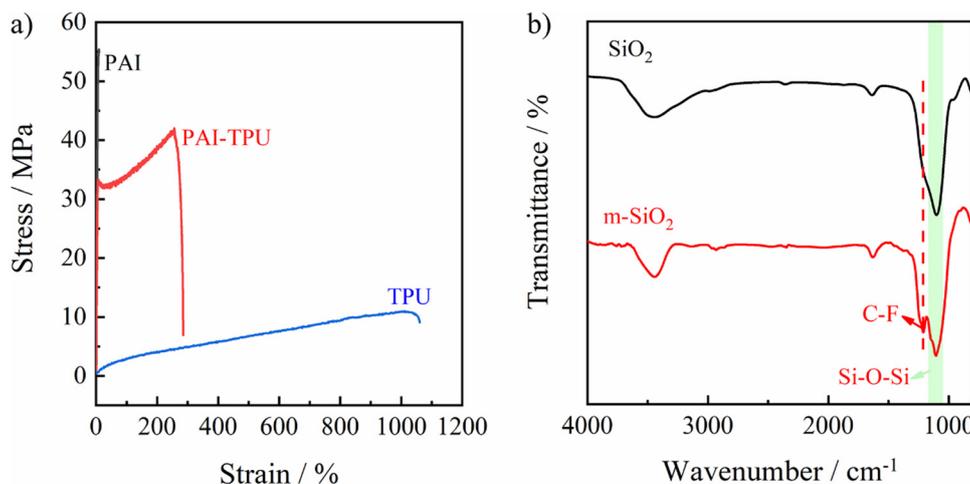


**Fig. 1** Mechanical curves of PAI (black line), PAI–TPU stretchable substrate (red line) and TPU (blue line) films (a). FTIR curves of $SiO_2$ (black line) and $m-SiO_2$ (red line).

of beyond 40 MPa and an elongation at break of approaching 300%. It should be noted that although some poly(amide–imide–urethane) thermoplastic elastomers have been reported, which exhibit a large elongation at break, the rigidity (tensile strength) of poly(amide–imide–urethane) is much lower than that of the TPU–PAI substrate.[31,32] More importantly, the rigidity and flexibility of the PAI–TPU substrate is controllable by varying the ratio of TPU to PAI due to the high compatibility between PAI and TPU. For the superhydrophobic coating, a silane coupling agent named FAS-17 containing fluorinated alkyl chains was grafted on the surface of $SiO_2$ nanoparticles. The successful modification was verified by FTIR results as shown in Fig. 1b, in which a new absorption band at 1210 cm$^{-1}$ ascribed to the C–F stretching vibration of –$CF_3$ and –$CF_2$– groups appeared for the modified $SiO_2$ (m-$SiO_2$).[33–35] Furthermore, the weight fraction of FAS-17 grafted onto the $SiO_2$ was investigated. $SiO_2$ exhibited a negligible weight loss with increasing temperature up to 800 °C as shown in Fig. S4 (ESI†), while the weight loss of m-$SiO_2$ sharply increased to 23.7 wt%, confirming again that the silane coupling agent was grafted onto the surface of $SiO_2$. Obviously, FAS-17 can be completely evaporated during the heating process because of its relatively low boiling point (around 230 °C). Therefore, the weight fraction of FAS-17 grafted on the $SiO_2$ surface can be calculated from the following eqn (1).

$$w = (\gamma_1 - \gamma_2)/\gamma_1 \qquad (1)$$

where $w$ is the weight fraction of FAS-17 grafted onto the surface of $SiO_2$. $\gamma_1$ and $\gamma_2$ are the char yields of $SiO_2$ and m-$SiO_2$, respectively. By calculation, $w$ is estimated to be around 24 wt%, demonstrating sufficient fluorinated alkyl chains are attached to $SiO_2$ surfaces, which is good for decreasing the surface energy of the $SiO_2$ nanoparticles. It should be noted that although FAS-17 has been widely used in various areas due to its unique properties such as high chemical and thermal stability, the use of fluoride would involve environmental problems. Therefore, optimization of this work has been performed

to reduce the usage or replace the fluorinated coupling agent. In more detail, the silica microcapsule was realized by hydrolysis and condensation of tetraethyl orthosilicate (TEOS) using an aqueous glycerol micro-emulsion as the template. Through adjusting the parameters, the size of the silica microcapsules can be varied to control the surface roughness. After spraying the silica microcapsules onto the PAI–TPU substrate, the primer coating was immersed into polydimethylsiloxane (PDMS) solution to form a protective layer. The mechanical robustness and durability of this superhydrophobic surface is being evaluated.

To strength the mechanical robustness of the stretchable superhydrophobic surface, TPU was selectively adopted to anchor m-$SiO_2$ in the superhydrophobic layer. It is found that the surface energy of TPU (13.3 mJ m$^{-2}$) is higher than that of m-$SiO_2$ (0.49 mJ m$^{-2}$), but lower than that of PAI (23.1 mJ m$^{-2}$). It is believed that m-$SiO_2$ would float up and TPU would sink down in the superhydrophobic coating layer while TPU would float up and PAI sink down in the PAI–TPU flexible substrate layer because of their differences in surface energy.[36] Indeed, in the FTIR spectrum of the PAI–TPU/m-$SiO_2$ stretchable superhydrophobic film as shown in Fig. 2a, the Si–O–Si characteristic peak at 1091 cm$^{-1}$ and C–F stretching vibration peak at 1203 cm$^{-1}$ ascribed to m-$SiO_2$ were maintained. On the other hand, the N–H characteristic peaks at 1532 and 3326 cm$^{-1}$ ascribed to TPU disappeared after spraying m-$SiO_2$ decorated with TPU, suggesting the stretchable superhydrophobic surface was occupied by m-$SiO_2$. In other words, the TPU in the superhydrophobic coating layer sank down, and entangled with the TPU in the PAI–TPU stretchable substrate during the evaporating process of the solvent. As a result, the compatibility between the modified silica and polymer substrate can be improved due to the same component of TPU in the superhydrophobic layer and stretchable substrate layer, which is helpful for obtaining good mechanical properties as discussed later. This self-assembly was also verified by XPS. As show in Fig. 2b, the XPS measurement supported the appearance of C, O, F, and Si from m-$SiO_2$, but the characteristic peak of N from
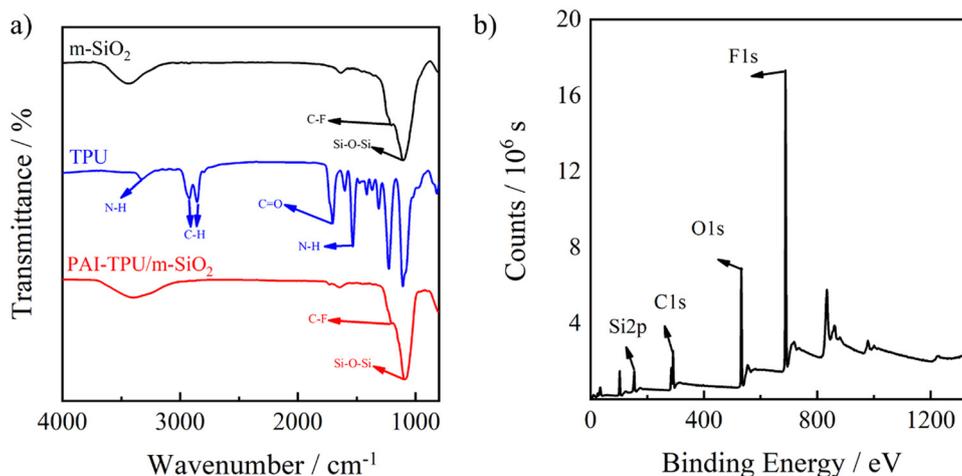


**Fig. 2** FTIR spectra of m-$SiO_2$ (black line), TPU (blue line), and PAI–TPU/m-$SiO_2$ stretchable (red line) surfaces (a). XPS spectrum of PAI–TPU/m-$SiO_2$ stretchable superhydrophobic film (b).
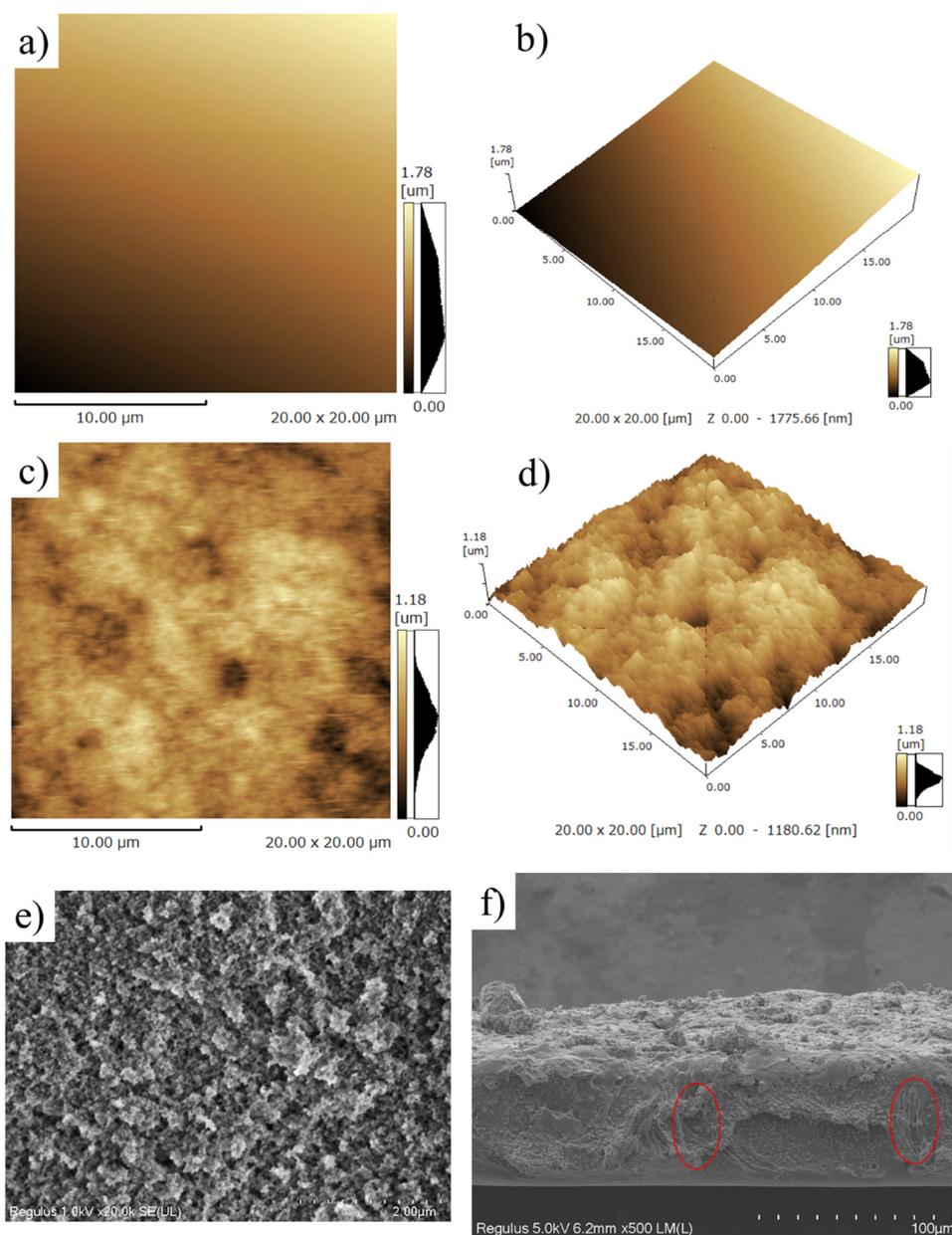
TPU was not found. Furthermore, integrated peak intensities indicated atomic ratios of 40/12/20/28 for F/Si/O/C on the PAI–TPU/m-SiO$_2$ stretchable superhydrophobic surface, and the Si weight ratio of 19.2 wt% calculated from XPS was higher than that of 13 wt% derived from TGA of m-SiO$_2$ decorated with TPU, suggesting again that the m-SiO$_2$ floated up during the self-assembly. It is believed that the self-assembly favored the construction of a hierarchical porous structure for the superhydrophobic surface with good robustness as will be discussed later.

## 2.2 Surface morphology and wetting behavior

The morphology of the superhydrophobic surface was firstly investigated using atomic force microscopy (AFM). As shown in Fig. 3a and b, the surface of the PAI–TPU substrate is quite smooth, with a root mean square ($R_q$) of 27 nm. After spraying m-SiO$_2$ nanoparticles, the $R_q$ sharply increased to 163.6 nm for the PAI–TPU/m-SiO$_2$ surface as shown in Fig. 3c. Moreover, many micro-sized wavy ridges and caves were observed in the AFM 3D image as shown in Fig. 3d. The unique structure allows for air pockets to be located under the surface of water droplets, and promotes the formation of liquid–air–solid interfaces. It has been reported that the air layer can protect the surface roughness of superhydrophobic surfaces, and thus improve the durability of the superhydrophobic surface.[37–39] This unique hierarchical porous structure was also observed by SEM. More specifically, these wavy ridges constructed coral-shaped



**Fig. 3** Atomic force microscopy 2D (a, c) and 3D (b, d) pictures of the PAI–TPU substrate (a, b) and PAI–TPU/m-SiO$_2$ stretchable superhydrophobic surface (c, d). Scanning electron microscopy images of surface (e) and cross-section (f) of the PAI–TPU/m-SiO$_2$ stretchable superhydrophobic surface.

structures during the self-assembly process as shown in Fig. 3e. In addition, the EDS elemental mapping exhibited that the four elements of C, O, Si, F were distributed uniformly on the surface of the PAI–TPU/m-SiO$_2$ film as shown in Fig. S5 (ESI†), suggesting that the micro/nano hierarchical porous structures were located uniformly on the stretchable superhydrophobic surface. In other words, the whole surface of the PAI–TPU/m-SiO$_2$ stretchable film has the same superhydrophobic characteristic. Furthermore, it should be noted that the superhydrophobic coating of m-SiO$_2$ was sprayed onto the wet substrate, meaning that the nanoparticles would be embedded into the stretchable PAI–TPU substrate. Indeed, as shown in Fig. 3f, m-SiO$_2$ was partially exposed to the air, and partially embedded in the polymer substrate. The unique morphology can further improve the durability of the super-hydrophobic surface, especially for mechanical robustness. However, it is well known that the interfacial force between inorganic nanoparticles and polymers is poor, and a superhydro-phobic coating would be pulled out of the substrate.[40] In this study, TPU as binder was adopted to be decorticated with m-SiO$_2$. More interestingly, the TPU also worked as a bridge, simulta-neously embracing m-SiO$_2$ nanoparticles and hooking the poly-mer substrate during the self-assembly process as shown in Fig. 3f (red circle), to strengthen the interfacial forces between the m-SiO$_2$ nanoparticles and PAI–TPU stretchable polymer substrate.

The PAI–TPU substrate showed a relatively lower water contact angle (CA) of 83° as shown in Fig. 4a; after spraying m-SiO$_2$, the CA sharply increased to 161° for the PAI–TPU/m-SiO$_2$ surface. To investigate the adhesion force between the PAI–TPU/m-SiO$_2$ stretchable surface and water, the sliding angle (SA) was investigated; the SA of the PAI–TPU/m-SiO$_2$ surface was as low as 1°, indicating a quite weak adhesion force between the PAI–TPU/m-SiO$_2$ superhydrophobic surface and water. In addition, as shown in Fig. 4b, the PAI–TPU/m-SiO$_2$ surface exhibited good resistance to commonly used liquids including orange juice, tea, milk, and coffee, suggesting that the PAI–TPU/m-SiO$_2$ stretchable superhydrophobic surface can be used in different environments. Fig. 4c shows a state diagram of the PAI–TPU/m-SiO$_2$ superhydrophobic coating immersed in deionized water. Many dense bubbles, similar to mirror glass, were formed on the superhydrophobic surface, which prevents water droplets from entering into the PAI–TPU/m-SiO$_2$ surface, and enhances the durability of the superhy-drophobic surface as discussed above. On the other hand, the contact area between the PAI–TPU/m-SiO$_2$ superhydrophobic surface and water droplets was quite small due to the layer of air trapped on the rough surface as shown in Fig. 4d, implying that the contact between the PAI–TPU/m-SiO$_2$ stretchable super-hydrophobic surface and water droplets is a Cassie state.[41–44] Moreover, the contact level of the PAI–TPU/m-SiO$_2$ superhydro-phobic surface with water droplets is much lower than that of the PAI–TPU polymer substrate with water droplets, which further demonstrates that the PAI–TPU/m-SiO$_2$ surface possesses
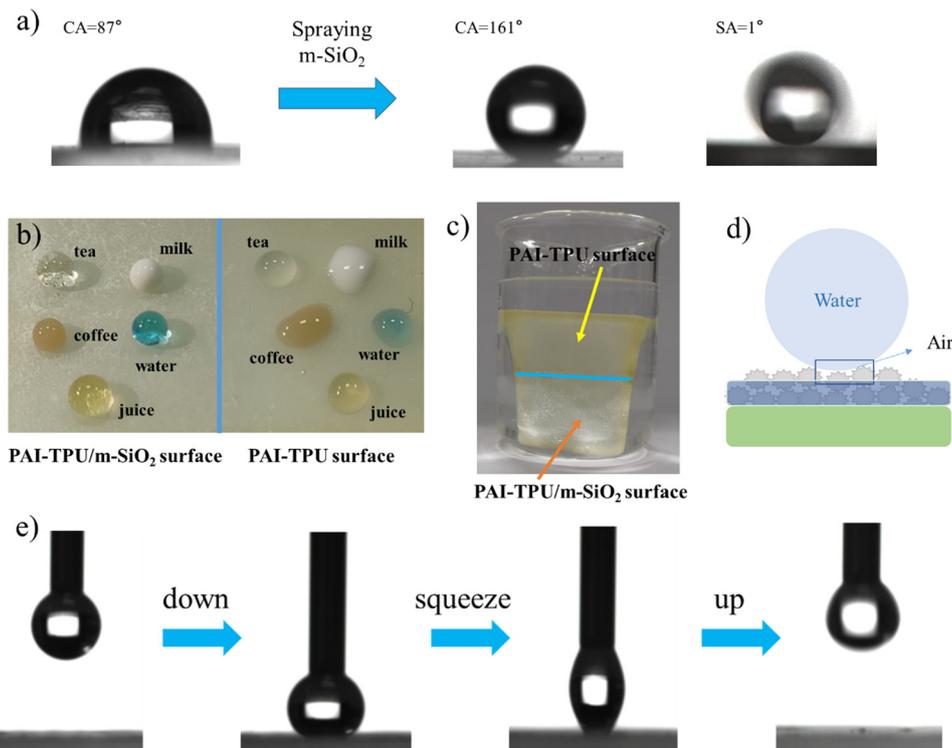


**Fig. 4** Optical pictures of water droplets placed on the PAI−TPU and PAI−TPU/m-SiO$_2$ surfaces (a). Wetting behavior of commonly used liquids on the surfaces of PAI−TPU/m-SiO$_2$ superhydrophobic coating and PAI−TPU substrate (b). PAI−TPU/m-SiO$_2$ superhydrophobic surface and PAI−TPU substrate were immersed in water (c). Schematic illustration of wetting behavior of the PAI−TPU/m-SiO$_2$ stretchable superhydrophobic surface (d). Optical pictures of squeezing test for the PAI−TPU/m-SiO$_2$ stretchable superhydrophobic surface using a syringe.

a much stronger repellency ability towards water and is more difficult to be wetted by water droplets. The stable Cassie contact was again confirmed by a squeezing test as shown in Fig. 4e. As expected, the water droplets stayed on the needle, and did not adhere to the PAI–TPU/m-SiO$_2$ superhydrophobic surface during the whole contacting–squeezing–repelling process.

### 2.3 Stretchable robustness

The flexibility of PAI–TPU/m-SiO$_2$ superhydrophobic films has been obviously enhanced, the tensile strength is as high as 41.4 MPa, at the same time, the elongation at break is approaching to 300% as shown in Fig. S6 (ESI†), suggesting the fabricated films can remain superhydrophobic even though they were suffering from a high load or extended by a long distance. For quantitative discussion on the stretchable performance, the wetting behavior of the PAI–TPU/m-SiO$_2$ surfaces was investigated under different strains. Encouragingly, water droplets still kept a spherical shape even though the strain on the PAI–TPU/m-SiO$_2$ superhydrophobic surface increased from 0 to 250% as shown in Fig. 5. In more detail, Fig. S7 (ESI†) shows

the change in CA and SA under different stretching strains. The CA and SA of the PAI–TPU/m-SiO$_2$ surface were respectively larger than 155° and less than 10° during the stretching process. Moreover, the water droplets immediately rolled away after they were placed on the stretched PAI–TPU/m-SiO$_2$ surface, suggesting the contact between the stretched PAI–TPU/m-SiO$_2$ surface and water drops is a Cassie state.[45] In order to make clear the origin of this excellent stretchable performance, AFM measurements were conducted to research the surface change under different strains. In the initial state, the PAI–TPU/m-SiO$_2$ superhydrophobic surface showed an $R_q$ of 187.4 nm, and the grooves were uniformly distributed on the surface. With increasing the strain from 50 to 250%, the $R_q$ increased from 239.7 to 545.9 nm correspondingly, and the size of the grooves became bigger and bigger but the neighboring m-SiO$_2$ nanoparticles were still interconnected with each other. In other words, the unique superhydrophobic structure was still kept after the stretching test.

The stretchable robustness of the PAI–TPU/m-SiO$_2$ superhydrophobic surface was further researched using the stretching–releasing test as shown in Fig. 6a. It is found that the CA
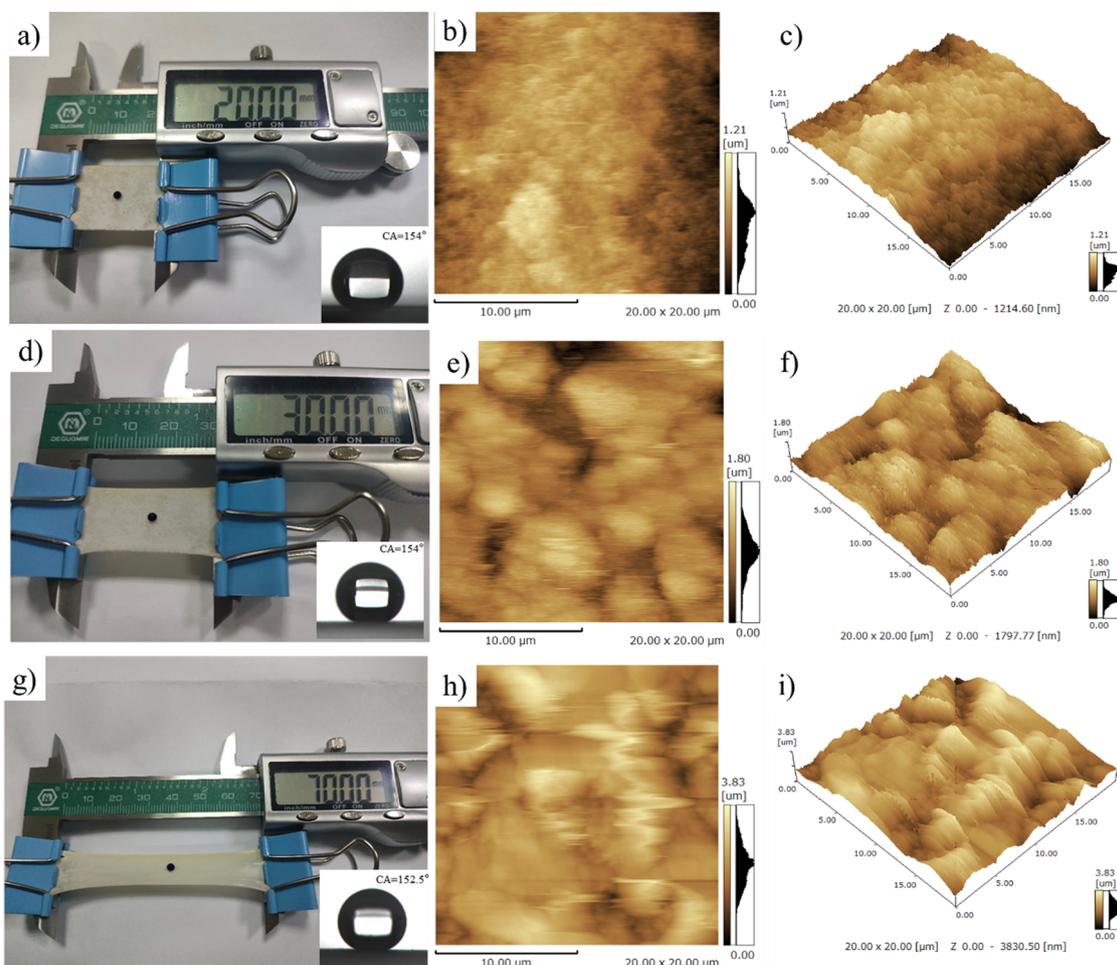


**Fig. 5** The wetting behavior of PAI–TPU/m-SiO$_2$ stretchable superhydrophobic surfaces with different elongations (0%: a; 50%: d; 250%: g). AFM 2D images of PAI–TPU/m-SiO$_2$ superhydrophobic surfaces with different elongations (0%: b; 50%: e; 250%: h). AFM 3D images of PAI–TPU/m-SiO$_2$ superhydrophobic surfaces with different elongations (0%: c; 50%: f; 250%: i).
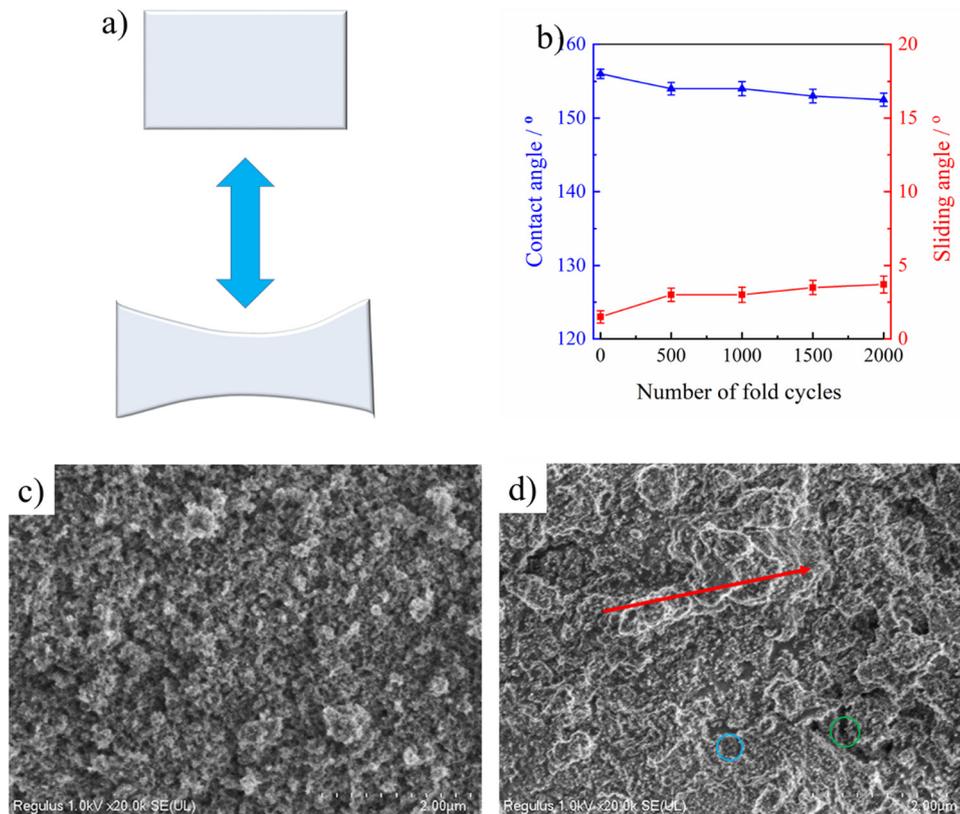
**Fig. 6** Schematic illustration of the stretching–releasing test (a). The change in CA and SA with increasing fold cycles (b). SEM pictures of PAI–TPU/m-SiO$_2$ stretchable superhydrophobic surface before (c) and after stretching–releasing test (d).

and SA were nearly unchanged after 2000 cycles of stretching–releasing with a strain of 30% as shown in Fig. 6b, suggesting the fabricated surface possessed excellent adaptability to distortion during the practical application. This unchanged wetting behavior is consistent with the well-preserved surface morphology. It is worth pointing out that compared with the morphology of the PAI–TPU/m-SiO$_2$ surface before stretching as shown in Fig. 6c, the well dispersed m-SiO$_2$ nanoparticles rearranged when the PAI–TPU/m-SiO$_2$ surface was stretched many times, and became closely aligned parallel to the strain direction (red arrow region) as shown in Fig. 6d. Interestingly, the orientation of the superhydrophobic nanoparticles under stretching did not damage the microscale open air pockets between micro-bulges (blue circle), and nanoscale sealed air pockets between nano-mastoids on the micro-bulges (green circle). These results demonstrated that the PAI–TPU/m-SiO$_2$ surface designed in this study is capable of remaining superhydrophobic even in the stretched state, suggesting that it can be used in flexible conditions that requires superhydrophobicity.

## 2.4 Mechanical robustness

To meet the requirements of practical usage, the fabricated superhydrophobic surfaces should keep a high level of water repellency even when they have suffered from mechanical deformation or damage. Firstly, ultrasonic treatment was adopted to evaluate the mechanical robustness of the PAI–

TPU/m-SiO$_2$ stretchable superhydrophobic surface as shown in Fig. 7a. In this study, the stretchable superhydrophobic surface was immersed in deionized water during the ultrasonic vibration with a frequency of 40 kHz and power of 50 W. It is obvious that such harsh ultrasonic treatment can easily damage fragile coatings. Encouragingly, as shown in Fig. 7b, a CA of beyond 150° and SA of below 5° were obtained for the PAI–TPU/m-SiO$_2$ stretchable superhydrophobic surface even when the treatment time was as long as 100 h, suggesting the interface forces are high enough to prevent the superhydrophobic coating of m-SiO$_2$ from peeling off from the stretchable substrate of PAI–TPU, and the m-SiO$_2$ nanoparticles were tightly bound with each other to prevent them from loosening. This is because the TPU decorated with m-SiO$_2$ not only works as a binder to hold m-SiO$_2$ together, but also works as a bridge to anchor m-SiO$_2$ closely into the PAI–TPU substrate as discussed above. Thus, the morphology was nearly unchanged, and the micro/nano hierarchical porous structure was preserved after ultrasonic treatment as shown in Fig. 7c. The excellent mechanical robustness was also confirmed using a sandpaper abrasion test as shown in Fig. 7d. The superhydrophobic surface was subjected to abrasion using 1200-grit sandpaper that was moved 5 cm in each cycle under a load of 100 g. The wetting behavior was plotted every 20 cycles. As shown in Fig. 7e, the CA and SA of the PAI–TPU/m-SiO$_2$ stretchable surface was nearly unchanged, the PAI–TPU/m-SiO$_2$ stretchable surface still remained superhydrophobic, and at the
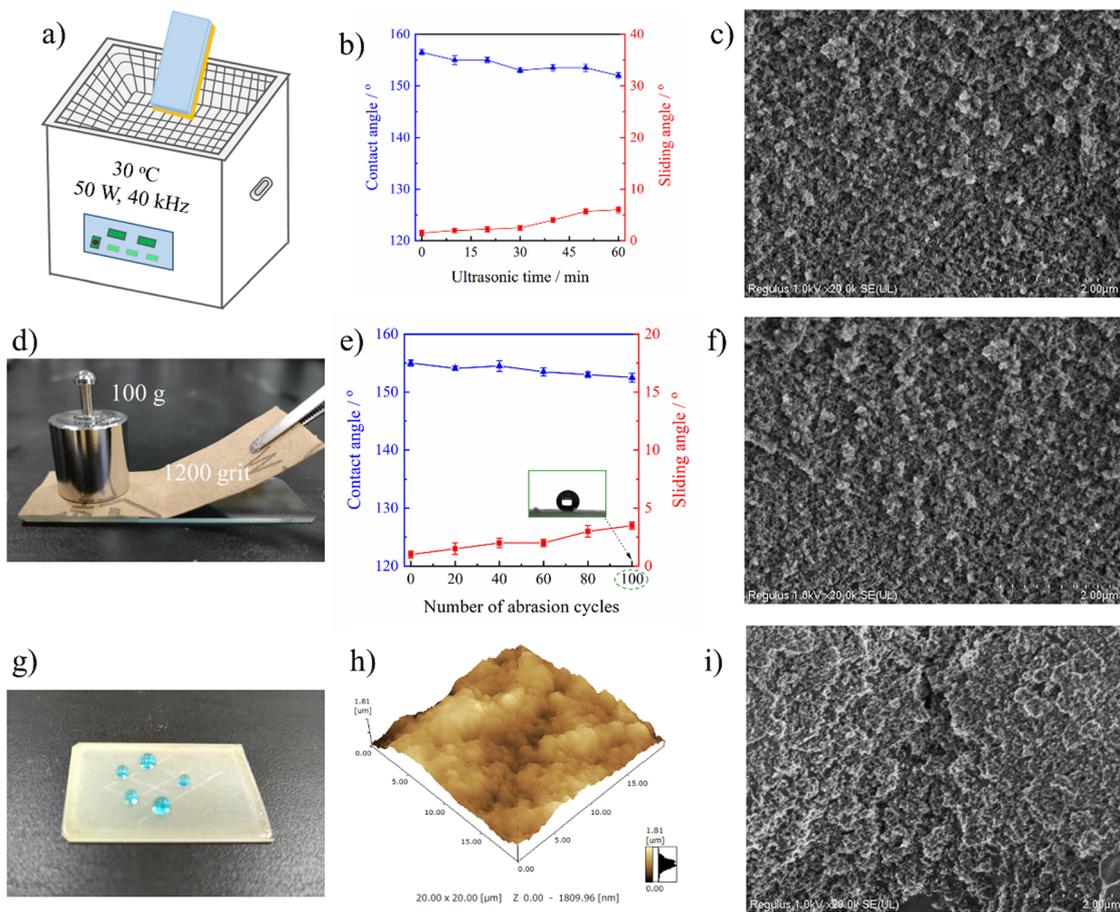
**Fig. 7** Schematic illustration of ultrasonic treatment (a). CA and SA as a function of time of ultrasonic treatment (b). SEM images after ultrasonic treatment (c), sandpaper abrasion test (f), and scratching by a knife (i). Photographic illustration of abrasion test (d). CA and SA as a function of abrasion cycles (e). Photograph illustrating the wetting behavior of water on scratched surface (g). AFM 3D (h) and SEM (i) images after scratching by a knife.

same time, the superhydrophobic micro/nano hierarchical porous structure was kept as shown in Fig. 7f. It is worth pointing out that even if the superhydrophobic coating was erased off when it was exposed to an external force, a much stronger protective layer would be formed by the m-SiO$_2$ nanoparticles embedded in the stretchable substrate. Indeed, as shown in Fig. 7g, the PAI–TPU/m-SiO$_2$ superhydrophobic surface was scratched by a knife and a crack was clearly observed using AFM and SEM measurements as shown in Fig. 7h and i. However, the water drops on the cracks still exhibited spherical shapes. This is because the micro/nano hierarchical porous structure sealed inside the coating appeared, which continued to endow the PAI–TPU/m-SiO$_2$ surface with a distinguished superhydrophobic property and stable Cassie contact.

## 2.5 Thermal/cooling stability

Fig. 8a shows the wetting behavior of the stretchable PAI–TPU/m-SiO$_2$ surface with varying temperature in a wide range. Excitingly, this stretchable surface showed CA > 150° and SA < 10° even after it was heated at a temperature as high as 200 °C or cooled at −10 °C for 24 h. With further increasing to 250 °C, the superhydrophobicity was still maintained, but the stretchable PAI–TPU/m-SiO$_2$ film became yellow; this is because

the end group (amine group) of PAI is easily oxidized under such a high temperature. As shown in Fig. 8b, TGA was employed to reveal the reason for the unique thermal stability. It was found that weight-loss of the stretchable PAI–TPU/m-SiO$_2$ superhydrophobic surface barely happened due to the excellent thermal stability of the stretchable substrate. In fact, as shown in Fig. S8 (ESI†), the temperatures at 5% weight loss were found to be 428 °C for PAI, 338 °C for TPU, and 356 °C for the PAI–TPU substrate. The high thermal stability of PAI and TPU guaranteed the excellent thermal stability of the stretchable PAI–TPU/m-SiO$_2$ superhydrophobic surface.

Dynamic impalement resistance to hot-water flow is another issue for application of superhydrophobic surfaces.[46] Unfortunately, the dynamic impalement resistance of superhydrophobic surfaces is poor, especially for hot water, this is because the fragile hierarchical porous structure is easily damaged by the fast evaporation of hot water and the dramatic change in liquid surface tension.[47] In order to investigate this property, a splash experiment was designed. As shown in Fig. 8c, the distance between the beaker and PAI–TPU/m-SiO$_2$ surface is 15 cm, the angle between the horizontal base line and PAI–TPU/m-SiO$_2$ surface is 20°, and the wettability was measured after each splashing of 200 mL of boiling water. With increasing amount
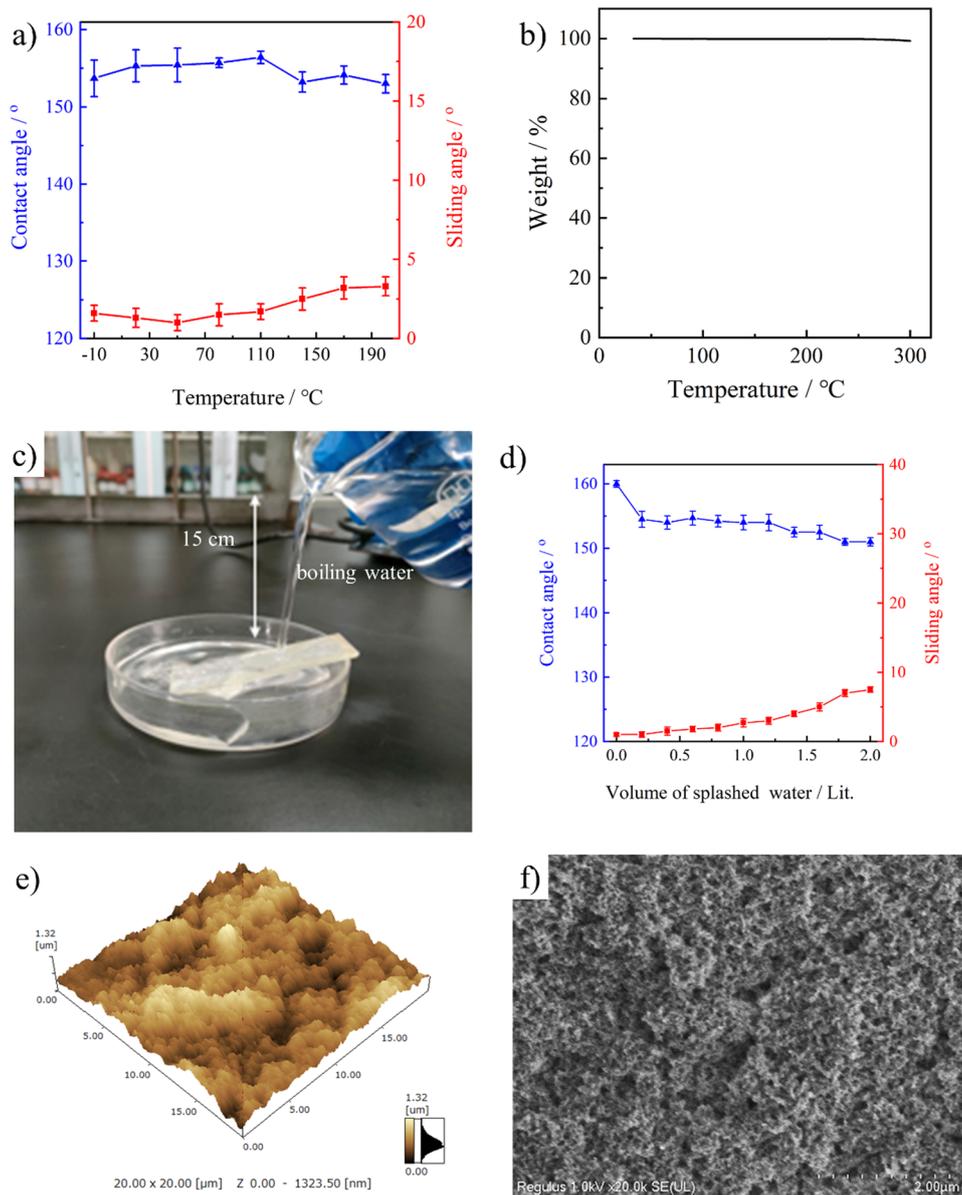
**Fig. 8** CA and SA as a function of temperature (a). TGA curve of the PAI–TPU/m-SiO$_2$ surface (b). Picture illustrating the impacting test (c). CA and SA as a function of the amount of impacting boiling water (d). AFM 3D (e) and SEM (f) images of the PAI–TPU/m-SiO$_2$ surface after the impacting test.

of splashing liquid up to 2000 mL, there was only a slight change in CA and SA, and the superhydrophobicity of the stretchable PAI–TPU/m-SiO$_2$ surface was still maintained as shown in Fig. 8d. The morphology after the impacting test was also investigated using AFM and SEM. As shown in Fig. 8e and f, the large roughness ($R_q$: 194 nm) and micro/nano superhydrophobic structure remained. These results demonstrated that the stretchable PAI–TPU/m-SiO$_2$ superhydrophobic surface possessed excellent dynamic impalement resistance.

### 2.6 UV durability and chemical stability

Another important issue is the UV resistance of superhydrophobic surfaces in consideration of outdoor applications; this is because organic components in superhydrophobic surfaces are prone to be oxidized and generate polar hydrophilic groups when they are exposed to UV radiation, which can change the wetting behavior of the superhydrophobic surface. As shown in Fig. 9a, the CA and SA were nearly unchanged even when the UV irradiation time is as long as 200 h under 150 W; the stretchable PAI–TPU/m-SiO$_2$ surface still kept the superhydrophobic property due to the UV resistant C–F and Si–O bonds.[48]

The chemical stability of a superhydrophobic surface has also been considered as one of the most important requirements for practical applications. In order to evaluate this property, firstly, water droplets with different pH were placed on the stretchable PAI–TPU/m-SiO$_2$ superhydrophobic surface. Interestingly, all the droplets showed a spherical shape independent of the pH value as shown in Fig. 9b. Furthermore, the
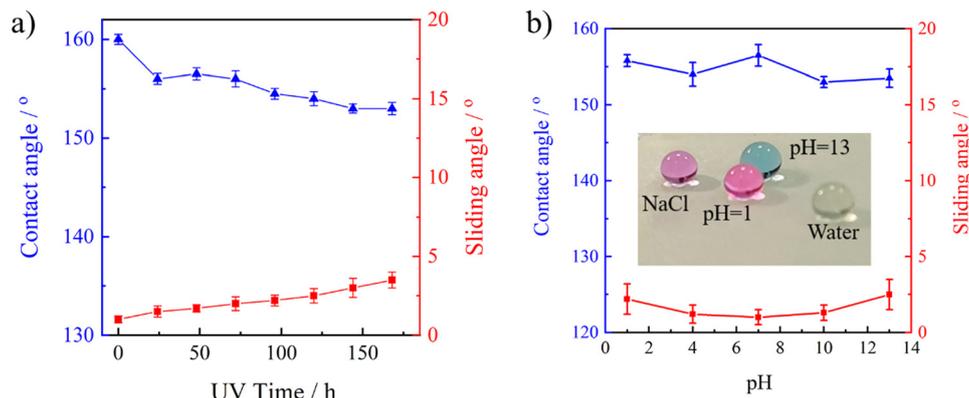
**Fig. 9** CA and SA as a function of UV irradiation time (a) and pH value (b); inset picture illustrates the wetting behavior at varying pH values.

stretchable PAI–TPU/m-SiO$_2$ superhydrophobic surface was placed into acid/base solutions, and the wetting behavior was measured to further evaluate the chemical stability of the PAI–TPU/m-SiO$_2$ superhydrophobic surface. Excitingly, the changes in CA and SA were almost negligible even when they were exposed to extreme acid/base solutions of pH = 1 or 13 for 6 h, and the CA was still larger than 150°, and the SA was below 5°. Also, the water droplets on the stretchable PAI–TPU/m-SiO$_2$ superhydrophobic surface still showed spherical shapes after such strong acid or alkali treatments. These results indicated that the stretchable superhydrophobic surface fabricated in this study was capable of resisting acid/alkali corrosions combining the advantages of air pocket structures and low surface energy.[49]

### 2.7 Self-healing capability

The self-healing capability of the stretchable PAI–TPU/m-SiO$_2$ superhydrophobic surface was evaluated by the change in wetting behavior before and after O$_2$ plasma etching and heating treatments. As shown in Fig. 10a, the CA of the PAI–TPU/m-SiO$_2$

superhydrophobic surface sharply decreased to 0° after O$_2$ plasma etching treatment, and became superhydrophilic. Encouragingly, the superhydrophobicity was recovered by heating treatment at 100 °C for 15 min as shown in Fig. 10a. This reversible transition between superhydrophobic and superhydrophilic indicated that the PAI–TPU/m-SiO$_2$ surface possessed a self-healing capability. Although the self-healing capability of superhydrophobic surfaces has been widely reported, the reason for this ability has been rarely studied in depth.[19,25] In general, the wetting behavior between water and the surface is mainly controlled by geometrical microstructures and chemical composition.[50] Firstly, AFM and SEM were used to research the changes in the morphology during the loss–recovery of the superhydrophobicity. As shown in Fig. 10b and c, the large roughness and micro/nano hierarchical porous structure were well preserved, suggesting the O$_2$ plasma etching treatment did not destroy the superhydrophobic structure. Nevertheless, it was reported that large rough and porous micro/nanostructures combined with attachment of polar groups could produce a synergistic effect on converting the wetting state.[51] Fig. 10d shows the change in chemical composition
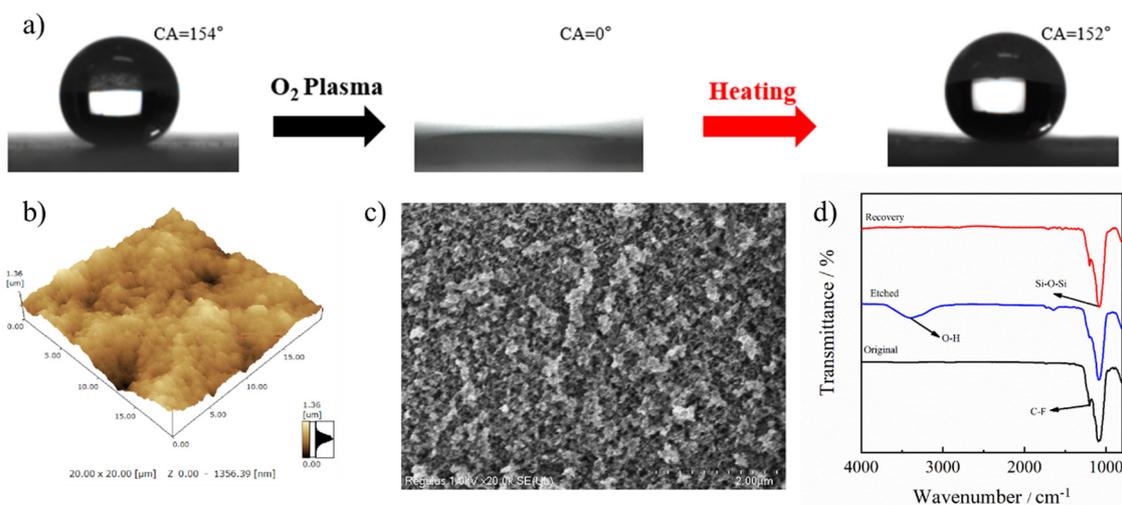


**Fig. 10** The effect of O$_2$ plasma etching and heating treatments on the wetting behavior of the stretchable PAI–TPU/m-SiO$_2$ superhydrophobic surface (a). AFM 3D (b) and SEM (c) pictures after O$_2$ plasma etching treatment. The FTIR spectra of the PAI–TPU/m-SiO$_2$ superhydrophobic surface before (black line) and after (blue line) O$_2$ plasma etching treatment, and after heating treatment (red line) (d).

derived from FTIR measurements. It is found that an obvious vibration peak at 3392 cm$^{-1}$ appeared after O$_2$ plasma treatment, suggesting O$_2$ plasma treatment brought hydrophilic polar groups of –OH or COOH onto the PAI–TPU/m-SiO$_2$ surface, which caused the transition from a superhydrophobic to a superhydrophilic surface. Interestingly, the signal at 3392 cm$^{-1}$ disappeared while the signal at 1202 cm$^{-1}$ became stronger after the heating treatment, suggesting that the heating treatment removed the hydrophilic polar groups while the hydrophobic group (fluorocarbon bond) migrated to the top surface of PAI–TPU/m-SiO$_2$ due to the low surface energy of m-SiO$_2$, and thus the superhydrophobicity of the PAI–TPU/m-SiO$_2$ surface was recovered.

## 2.8 Icephobic property

Icephobic surfaces have been attracting more and more attention in many areas such as aircraft, power lines, and so on.[52] In general, freezing water droplets contains two phases: the precooling phase and ice growth phase. Firstly, the time of performing the precooling phase $\Delta t_{precooling}$ can be calculated using eqn (2) from a macroscopic viewpoint:[53]

$$\Delta t_{precooling} = (\rho_w C_w \Delta T)/q \qquad (2)$$

where $\rho_w$ and $C_w$ are the density and specific heat of water, respectively. $\Delta T$ is the temperature change of the water droplet, and $q$ is the heat transfer cooling rate per unit mass. On the other hand, the time required to perform the growth phase $\Delta t_{ice\ growth}$ can be calculated using eqn (3):

$$\Delta t_{ice\ growth} = (\rho_w \Delta H)/q \qquad (3)$$

where $\Delta H$ is the enthalpy change of the water droplet. Obviously, the time for freezing the water droplet is primarily controlled dominated by the heat transfer rate. In other words, the freezing process can be delayed by reducing the heat transfer rate between the liquid droplet and contacting surface.

In order to discuss the icephobic property of the PAI–TPU/m-SiO$_2$ superhydrophobic surface, the icing delay test was conducted by respectively laying water droplets on the stretchable PAI–TPU/m-SiO$_2$ superhydrophobic and PAI–TPU substrate surfaces, where these surfaces were precooled and maintained at −20 °C. Firstly, the precooling phase immediately started after the droplet was placed on these cold surfaces. And then the ice growth phase started, and the freezing front propagated from the cold surface to the tip of the droplet. It is found that the PAI–TPU substrate and PAI–TPU/m-SiO$_2$ superhydrophobic surface exhibited similar patterns, but the duration of the precooling phase and the speed of the freezing front significantly varied. The stretchable PAI–TPU/m-SiO$_2$ superhydrophobic surface was capable of causing a huge delay ($\sim$385 s) in this freezing process, and icing time is nearly 6 times that of the PAI–TPU substrate ($\sim$65 s). As shown in Fig. 4, the stretchable PAI–TPU/m-SiO$_2$ superhydrophobic surface and PAI–TPU substrate respectively showed CA values of 161° and 87°, the higher CA can reduce the contact area between the water droplet and cold surface, resulting in a decreased heat transfer rate. Furthermore, the micro/nano hierarchical porous structure of the stretchable PAI–TPU/m-SiO$_2$ superhydrophobic surface also can decrease the heat

transfer rate.[54] In fact, there were plenty of air traps in the micro/nano hierarchical structure of the PAI–TPU/m-SiO$_2$ superhydrophobic surface as discussed above; in other words, the water droplets were laid on a hybrid surface composed of solid and air. The icing delay mechanism of the PAI–TPU/m-SiO$_2$ superhydrophobic surface was further quantitatively discussed by calculating the ratio of trapped air in the superhydrophobic structure using the Cassie–Baxter equation (eqn (4)):[55]

$$\cos\theta = f_b(\cos\theta_b + 1) - 1 \qquad (4)$$

where $\theta$ is the water contact angle of the PAI–TPU substrate and PAI–TPU/m-SiO$_2$ superhydrophobic surface, $\theta_b$ (40°) is the CA of the liquid droplet on the glass, $f_b$ is the surface ratio under the non-wetting state. Before spraying m-SiO$_2$, the PAI–TPU substrate showed a relatively lower $\theta$ of 83°, the area ratio of trapped air between the water droplets and PAI–TPU substrate was 36.5% ($1 - f_b$). After spraying m-SiO$_2$ onto the PAI–TPU substrate, the $\theta$ of the PAI–TPU/m-SiO$_2$ surface increased to 165°, and the proportion of air captured area significantly increased to 98%. Therefore, the above analysis further supported that the micro/nano hierarchical porous structure produced during self-assembly is the key to the icephobic property of the stretchable PAI–TPU/m-SiO$_2$ superhydrophobic surface.

It has been reported that the superhydrophobic property would be lost during the icing/deicing process owing to the fragile hierarchical porous structure.[56] Herein the wetting behavior of the stretchable PAI–TPU/m-SiO$_2$ superhydrophobic surface was investigated in every cycle of the icing/deicing treatment. The CA and SA were respectively investigated to be 154° and 3° after five cycles of the icing/deicing process as shown in Fig. 11a, indicating the superhydrophobic characteristic of the stretchable PAI–TPU/m-SiO$_2$ surface was not lost. Furthermore, the morphology of the PAI–TPU/m-SiO$_2$ surface after the icing/deicing test was also researched. The hierarchical porous and clustered-like structures were kept as shown in Fig. 11b. These results proved the importance of the self-assembly again.

## 2.9 Anti-fouling and self-cleaning properties

The anti-fouling ability of the stretchable PAI–TPU/m-SiO$_2$ superhydrophobic surface is presented in Fig. 12. Firstly, the fabricated surface was placed into a dye solution as shown in Fig. 12a. Interestingly, the surface remained clean and free of any contamination when it was taken out from the solution. Fig. 12b exhibits pictures of water droplets on the PAI–TPU/m-SiO$_2$ surface contaminated with carbon black: the water droplet collected the particles, and rolled across the PAI–TPU/m-SiO$_2$ surface even when the superhydrophobic surface was scuffed by a knife. These results indicated that the PAI–TPU/m-SiO$_2$ superhydrophobic surface possesses excellent antifouling and self-cleaning properties. In addition, the stretchable PAI–TPU/m-SiO$_2$ superhydrophobic surface can be uniformly attached to objects with different curvatures or shapes. For example, a PAI–TPU/m-SiO$_2$ superhydrophobic surface was closely attached to an index finger, and it could still retain low-adhesive capability even under bending/stretching as shown in Fig. 12c. Excellent
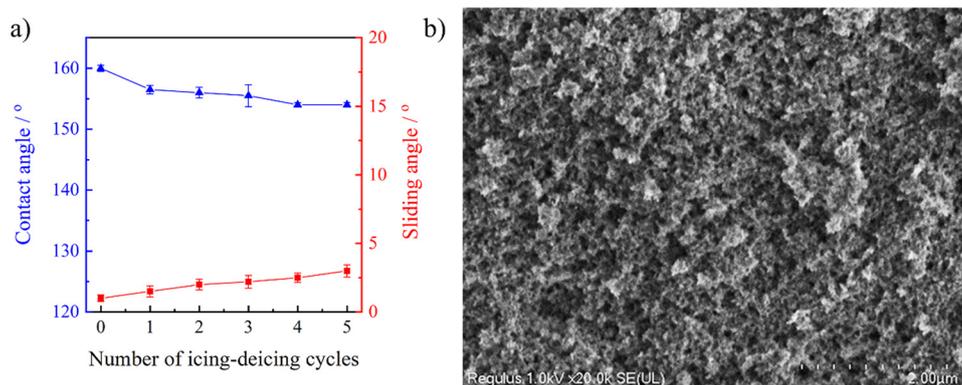
**Fig. 11** The effect of icing/deicing treatment on the wetting behavior of the stretchable PAI−TPU/m-SiO$_2$ superhydrophobic surface (a). SEM picture of the stretchable PAI−TPU/m-SiO$_2$ superhydrophobic surface after five cycles of icing/deicing treatment (b).
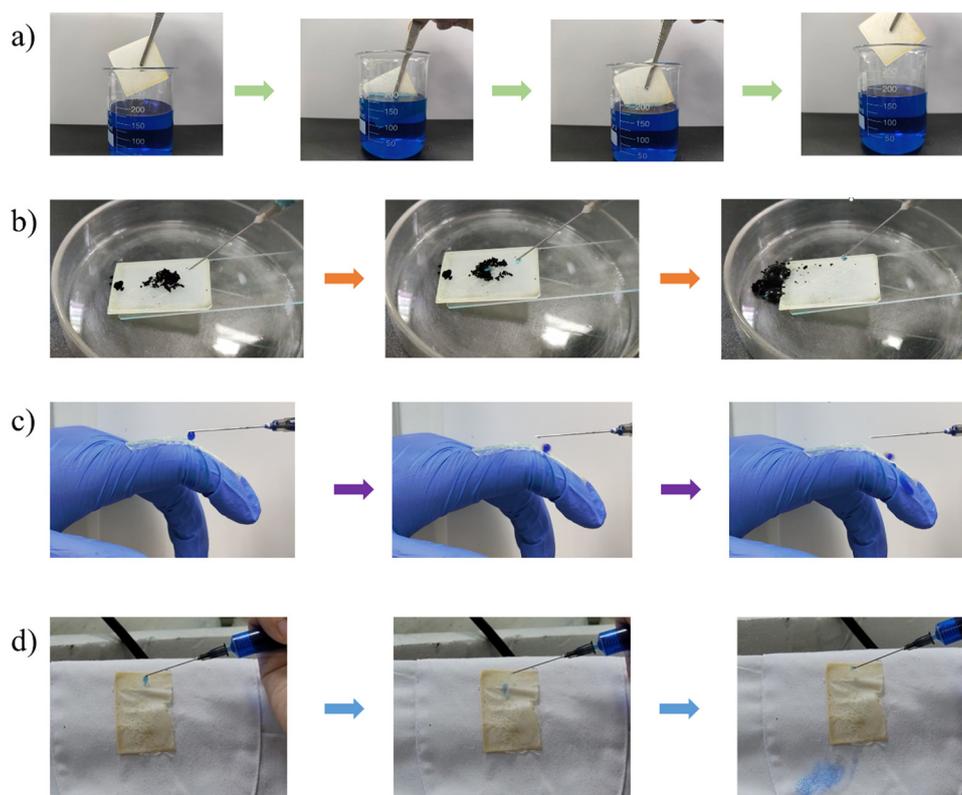


**Fig. 12** The immersed and lifted-out behaviors of the PAI−TPU/m-SiO$_2$ surface in a blue dye solution of water (a). Self-cleaning test of the scuffed PAI−TPU/m-SiO$_2$ superhydrophobic surface (b). The wetting behavior of the stretchable PAI−TPU/m-SiO$_2$ superhydrophobic surface attached to an index finger (c) and lab coat (d).

water repellency was observed when monitoring a water jet directed toward the film. Fig. 12d further reveals that the stretchable PAI−TPU/m-SiO$_2$ superhydrophobic surface can be adapted to double-sided adhesive tape, suggesting the superhydrophobic surface prepared in this study can be applied to an irregular surface. Moreover, the loaded droplets (blue dyed water) rapidly rolled across the superhydrophobic area while the uncovered area was wetted. These results demonstrated that the PAI−TPU/m-SiO$_2$ superhydrophobic surface could be applied to irregular morphologies with bending/stretching capability.

## 3. Conclusion

In summary, a simple method was proposed to construct hierarchical porous structures for superhydrophobic surfaces by self-assembly. By delicately utilizing the surface energy differences of a superhydrophobic coating of m-SiO$_2$ and

polymer substrate of PAI and TPU, m-SiO$_2$ was tightly attached to the stretchable substrate of PAI–TPU by the bridge effect of TPU. As expected, the PAI–TPU/m-SiO$_2$ surface still remained superhydrophobic even after it was exposed to lots of stability tests such as sandpaper abrasion, knife-scuffing, ultrasonic treatment, and hot-water jet impact, acid–base immersing, cooling or heating, and UV irradiation. Furthermore, the PAI–TPU/m-SiO$_2$ surface possessed excellent self-healing and icephobic properties. Through controlling the ratio of TPU in the polymer substrate, the stretchable film exhibited water repellency even after it was subjected to a high strain of 250%, or under a periodical linear stretching of 30% for 2000 cycles. For practical application, PAI–TPU/m-SiO$_2$ superhydrophobic films were applied as water-proof covers for complex/curved surfaces, or served as self-cleaning coatings. It should also be pointed out that the approach is capable of producing stretchable superhydrophobic films in large-scale by the simple spray method. Due to the unique durability, simple methodology, and excellent multi-functionality, we believe that the methodology performed in this work can be promising not only to the burgeoning wearable electronics field, but also to complex conditions where it is required to simultaneously address the stability and adaptability.

## Author contributions

The manuscript was written through contributions of all authors. All authors have given approval to the final version of the manuscript. S. H. and I. N. contributed equally to this work.

## Conflicts of interest

The authors declare no competing financial interest.

## Acknowledgements

## References

1  A. Kumar, V. Mishra, S. Negi and S. Kar, *J. Coat. Technol. Res.*, 2023, **20**, 1499–1512.

2  A. Aparna, A. S. Sethulekshmi, A. Saritha and K. Joseph, *Prog. Org. Coat.*, 2022, **166**, 106819.

3  S. G. Moghadam, H. Parsimehr and A. Ehsani, *Adv. Colloid Interface Sci.*, 2021, **290**, 102397.

4  A. Davis, S. Surdo, G. Caputo, I. S. Bayer and A. Athanassiou, *ACS Appl. Mater. Interfaces*, 2018, **10**, 2907–2917.

5  B. Li, J. C. Luo, X. W. Huang, L. W. Lin, L. Wang, M. J. Hu, L. C. Tang, H. G. Xue, J. F. Gao and Y. W. Mai, *Composites, Part B*, 2020, **181**, 107580.

6  S. L. Wang, X. Q. Yu and Y. F. Zhang, *J. Mater. Chem. A*, 2017, **5**, 23489–23496.

7  Y. S. Li, H. Shao, P. F. Lv, C. Y. Tang, Z. K. He, Y. L. Zhou, M. B. Shuai, J. Mei and W. M. Lau, *Chem. Eng. J.*, 2018, **338**, 440–449.

8  A. M. Rather and U. Manna, *J. Mater. Chem. A*, 2017, **5**, 15208–15216.

9  O. Erdene-Ochir, V. T. Do and D. M. Chun, *Polymer*, 2022, **255**, 125158.

10  M. Rutkevicius, T. Pirzada, M. Geiger and S. A. Khan, *J. Colloid Interface Sci.*, 2021, **596**, 479–492.

11  S. Foorginezhad and M. M. Zerafat, *Appl. Surf. Sci.*, 2019, **464**, 458–471.

12  Y. Aleeva, V. Ferrara, A. Bonasera, D. C. Martino and B. Pignataro, *Colloids Surf., A*, 2021, **631**, 127633.

13  Z. H. Chen, X. J. Su, W. J. Wu, S. T. Chen, X. F. Zhang, Y. H. Wu, H. L. Xie and K. Q. Li, *Surf. Coat. Technol.*, 2022, **434**, 128182.

14  R. Y. Sun, J. Zhao, J. L. Mo, N. K. Yu and Z. R. Zhou, *Mater. Sci. Eng., B*, 2023, **288**, 116144.

15  B. John, P. R. Rajimol, T. P. D. Rajan and S. K. Sahoo, *Surf. Coat. Technol.*, 2022, **451**, 129036.

16  Y. Bao, H. Yang, L. Gao, X. Zheng, X. J. Shi, W. B. Zhang and C. Liu, *Sol. Energy Mater. Sol. Cells*, 2022, **245**, 111838.

17  C. Ke, Z. F. Li, C. H. Zhang, X. G. Wu, Z. P. Zhu and Y. D. Jiang, *Coatings*, 2021, **11**, 174.

18  X. W. Huang, B. Li, X. Song, L. Wang, Y. Shi, M. J. Hu, J. F. Gao and H. G. Xue, *J. Ind. Eng. Chem.*, 2019, **70**, 243–252.

19  T. Verho, C. Bower, P. Andrew, S. Franssila, O. Ikkala and R. H. A. Ras, *Adv. Mater.*, 2011, **23**, 673–678.

20  Y. H. Teng, Y. F. Wang, B. Y. Shi and Y. Z. Chen, *Prog. Org. Coat.*, 2020, **147**, 105877.

21  Z. Y. Dai, G. Chen, S. Ding, J. Lin, S. B. Li, Y. Xu and B. P. Zhou, *Adv. Funct. Mater.*, 2021, **31**, 2008574.

22  M. K. Kim, W. H. Yao and Y. R. Cho, *Colloids Surf., A*, 2022, **634**, 127973.

23  N. Celik, I. Torun, M. Ruzi, A. Esidir and M. S. Onses, *Chem. Eng. J.*, 2020, **396**, 125230.

24  X. Hu, C. Y. Tang, Z. K. He, H. Shao, K. Q. Xu, J. Mei and W. M. Lau, *Small*, 2017, **13**, 1602353.

25  A. M. Atta, A. O. Ezzat, A. M. El-Saeed, M. H. Wahby and M. M. S. Abdallah, *Prog. Org. Coat.*, 2020, **140**, 105502.

26  Z. Fan, Y. Wang, J. Jeon, H. D. Kim, Y. Fang, X. Shi, Z. Luo, H. Ohkita and B. Wang, *Surf. Interfaces*, 2022, **32**, 102130.

27  T. J. Murray, *Macromol. Mater. Eng.*, 2008, **293**, 350–360.

28  J. M. Dodda and P. Belsky, *Eur. Polym. J.*, 2016, **84**, 514–537.

29  S. H. Hou, I. Noh, X. L. Shi, Y. B. Wang, H. Do Kim, H. Ohkita and B. B. Wang, *Colloids Surf., A*, 2023, **664**, 131181.

30  J. M. Garcia, F. C. Garcia, F. Serna and J. L. de la Pena, *Prog. Polym. Sci.*, 2010, **35**, 623–686.

31  Y. F. Guo, A. M. Cristadoro, J. Kleemann, S. Bokern, R. P. Sijbesma and Z. Tomovic, *ACS Appl. Polym. Mater.*, 2023, **5**, 4517–4524.

32  T. L. Wang and F. J. Huang, *Polym. Int.*, 1998, **46**, 280–284.

© 2023 The Author(s). Published by the Royal Society of Chemistry

33 Y. W. Wang, B. L. Ou, P. Zhu, B. Niu, Y. Guo and Q. Zhi, *Surf. Interfaces*, 2022, **29**, 101747.

34 D. K. Li, X. L. Gou, D. H. Wu and Z. G. Guo, *Nanoscale*, 2018, **10**, 6695–6703.

35 S. S. Jia, S. L. Deng, S. Luo, Y. Qing, N. Yan and Y. Q. Wu, *Appl. Surf. Sci.*, 2019, **466**, 84–91.

36 S. H. Joghee, K. M. Uthandi, N. Singh, S. Katti, P. Kumar, R. K. Renganayagalu and B. Pullithadathil, *Langmuir*, 2020, **36**, 6352–6364.

37 J. F. Xu, X. L. Deng, Y. Y. Dong, Z. Z. Zhou, Y. L. Zhang, J. P. Yu, J. C. Cai and Y. X. Zhang, *Carbohydr. Polym.*, 2020, **247**, 116694.

38 W. K. Lee and T. W. Odom, *ACS Nano*, 2019, **13**, 6170–6177.

39 Y. Q. Wang, Y. Shi, L. J. Pan, M. Yang, L. L. Peng, S. Zong, Y. Shi and G. H. Yu, *Nano Lett.*, 2014, **14**, 4803–4809.

40 Z. F. Chen, G. J. Li, L. Y. Wang, Y. L. Lin and W. Zhou, *Mater. Des.*, 2018, **141**, 37–47.

41 T. H. Yang, M. Wang, X. Wang, X. Di, C. Y. Wang and Y. D. Li, *Soft Matter*, 2020, **16**, 3678–3685.

42 J. X. Zhao, S. S. Chen, W. L. Su, L. Zhu, X. Cheng, J. L. Wu, S. G. Zhao and C. J. Zhou, *Thin Solid Films*, 2021, **717**, 138467.

43 T. P. Rasitha, S. C. Vanithakumari, D. N. G. Krishna, R. P. George, R. Srinivasan and J. Philip, *Prog. Org. Coat.*, 2022, **162**, 106560.

44 S. M. Lim, J. Ryu, E. H. Sohn, S. G. Lee, I. J. Park, J. Hong and H. S. Kang, *ACS Appl. Mater. Interfaces*, 2022, **14**, 10825–10835.

45 K. Liu, C. Yang, L. H. Song, Y. Wang, Q. Wei, Alamusi, Q. B. Deng and N. Hu, *Compos. Sci. Technol.*, 2022, **218**, 109148.

46 H. Zhou, X. S. Jing and Z. G. Guo, *Nanoscale Adv.*, 2020, **2**, 1473–1482.

47 Y. Y. Liu, X. Q. Chen and J. H. Xin, *J. Mater. Chem.*, 2009, **19**, 5602–5611.

48 A. Gharieh and M. Pourghasem, *Polym. Adv. Technol.*, 2022, **33**, 3312–3322.

49 F. Guo, Q. Y. Wen, Y. B. Peng and Z. G. Guo, *J. Colloid Interface Sci.*, 2017, **494**, 54–63.

50 M. Z. Khan, J. Militky, M. Petru, B. Tomkova, A. Ali, E. Toren and S. Perveen, *Eur. Polym. J.*, 2022, **178**, 111481.

51 W. L. Li, K. X. Liu, Y. X. Zhang, S. Guo, Z. X. Li and S. C. Tan, *Chem. Eng. J.*, 2022, **446**, 137195.

52 W. Huang, J. X. Huang, Z. G. Guo and W. M. Liu, *Adv. Colloid Interfaces*, 2022, **304**, 102658.

53 A. Elzaabalawy and S. A. Meguid, *Chem. Eng. J.*, 2022, **433**, 133637.

54 K. Maghsoudi, E. Vazirinasab, G. Momen and R. Jafari, *J. Mater. Process. Technol.*, 2021, **288**, 116883.

55 J. X. Zhang, L. G. Zhang and X. Gong, *Langmuir*, 2021, **37**, 6042–6051.

56 B. Subeshan, A. Usta and R. Asmatulu, *Surf. Interfaces*, 2020, **18**, 100429.